DOI 10.1515/polyeng-2012-0096 — J Polym Eng 2013; 33(5): 453–461

Jasbir S. Bedi, Daniel W. Lester, Yuan X. Fang, John F.C. Turner, John Zhou, Sulaiman M. Alfadul, Christopher Perry and Qiao Chen*

Electrospinning of poly(methyl methacrylate) nanofibers in a pump-free process

Abstract: The effects of processing parameters, including solution concentration, viscosity, nozzle diameter, voltage bias and the nozzle to collector distance, on the morphology and diameters of poly(methyl methacrylate) (PMMA) fibers have been systematically investigated, using a unique pump-free electrospinning method. For PMMA solution concentrations less than the critical entanglement concentration, c_e, prolate spheroid-shaped droplets or beads with fibers were formed, whereas at concentrations above c_e, good quality bead-free fibers were formed. Quantitative analysis revealed a linear dependence between the solution viscosity and fiber diameter. Larger fiber diameters were achieved by increasing the nozzle diameter and voltage bias. Increasing the bias voltage has the additional effect of broadening the diameter distribution, as a result of splaying and splitting. By contrast, when the strength of the electrical field was reduced by increasing the distance between the nozzle and collector, the overall fiber diameter was reduced.

Keywords: concentration; electrospinning; nanofiber; polymer; viscosity.

***Corresponding author: Qiao Chen,** Department of Chemistry, School of Life Sciences, University of Sussex, Brighton, BN1 9QJ, UK, e-mail: qiao.chen@sussex.ac.uk
Jasbir S. Bedi, Daniel W. Lester, Yuan X. Fang and John F.C. Turner: Department of Chemistry, School of Life Sciences, University of Sussex, Brighton, BN1 9QJ, UK
John Zhou: Department of Applied Sciences, London South Bank University, London SE1 0AA, UK
Sulaiman M. Alfadul: King Abdulaziz City for Science and Technology, P.O. Box 6086, Riyadh 11442, Saudi Arabia
Christopher Perry: Department of Basic Sciences, School of Medicine, Loma Linda University, Loma Linda, California 92350, USA

1 Introduction

Nanomaterials are intensely investigated because of their unique material properties, such as high surface-to-volume ratios and tunable optoelectronic properties on the nanometer scale. Amongst the different known nanoscaled morphologies, nanofibers have become the focus for immediate applications, due to their good mechanical strength, while maintaining high surface area to volume ratio. Prospective application areas for nanofibers include ion conductive nanofibrous membranes for high performance batteries [1], piezoelectric fibers [2], filtration [3], tissue engineering scaffolds [4], solar cells [5], and photocatalysts [6].

Electrospinning is a cost effective approach for producing polymers [7, 8] and metal oxide fibers [9]. In typical electrospinning processes [10], a high voltage is applied to a liquid drop, creating an electric field between the drop and a collector. The electrostatic repulsion counteracts the surface tension of liquid, which causes the droplet to stretch. At a critical point, a stream of liquid erupts from within the drop, forming a jet of fibers flowing away from the liquid drop followed by a series of electrically-driven bending instabilities.

Generally, the morphology of the fibers depends on various intrinsic and extrinsic parameters; the former parameters set are those that depend on the solution, whereas the latter are generally the processing parameters. Intrinsic parameters include solution viscosity, controlled by polymer molecular weight and concentration, surface tension, solvent vapor pressure, and diffusivity in air. Extrinsic or processing parameters include voltage bias, applied electric field strength, which depends on the tip-to-collector distance and bias voltage, nozzle orifice diameter, and solution feed rate [8, 11–17].

This work focused on controlling and understanding the formation and morphology of electrospun fibers. Determining the response of the distribution of the diameters of the electrospun fibers to the process parameters and polymer solution rheology is a challenging task, since many parameters are correlated to each other. This complexity is reflected in the number of inconsistent experimental results that have been previously reported.

For example, Katti et al. [17] reported that larger nozzle diameter resulted in larger fiber diameter, while

Macossay et al. [18] reported that the nozzle diameter has no influence on the fiber diameter. Although, it is generally agreed that larger bias voltage creates larger diameter fibers [19, 20], Katti et al. [17] reported that an increase in voltage caused a decrease in nanofiber diameter initially, but further increase caused nanofiber diameter fluctuation. More controversially, measurements taken by Gu et al. [21] showed no correlation between fiber diameter and bias voltage. We note that most of those reported results are obtained with flow-controlled electrospinning processes, in which the effects of the nozzle diameter and voltage bias could be affected by the solution pumping rate.

Such contradictory results suggest that there is complex interference between processing parameters and that previous experimental approaches have not disentangled these parameters sufficiently to allow a clear appraisal of the fundamental processes that occur in electrospinning. To avoid such complications and to eliminate any dependencies due to the pumping rate, we used a glass capillary with no extrinsic solution feed control, thus ensuring that the results of the electrospinning are determined by the strength of electrical field, nozzle diameters and solution viscosity alone. To our knowledge, the number of pump-free electrospinning studies is very limited [22], although there are clear technical advantages; for instance, a matrix of parallel nozzles can be used for high throughput production without cross interference between them, a potential consistency problem for flow-controlled electrospinning.

We chose PMMA in dimethylformamide (DMF) as a model system to examine the dependence of morphology of the nanofibers on the three isolated processing parameters mentioned above. PMMA nanofibers have wide potential applications in many areas, including tissue engineering [23], cell growth [24], and enzyme immobilization [25], due to their biocompatibility and adjustable hydrophilic/hydrophobic properties; they can also be used as templates for the formation of nanostructured metal oxides, such as TiO_2 [26]. As the morphology of these metal oxide nanostructures is directly determined by the PMMA nanostructure, a general and fundamental understanding of the dependence of nanomorphology on extrinsic processing parameters is highly important, if accurate and predictable control is to be achieved. Moreover, an optimized high throughput, pump-free electrospinning process could offer an opportunity for producing large quantities of metal oxide nanofibers as photocatalysts. In this study, we have identified the conditions for creating polymer fibers on the nanometer scale.

2 Experimental

The solutions used in the electrospinning experiments were prepared using PMMA with a weight average molecular weight of 996,000 g/mol, determined by gel permeation chromatography performed by the supplier (Sigma-Aldrich). The PMMA was used as received. PMMA was dissolved in DMF (Sigma Aldrich), forming solutions in concentrations ranging from 1 to 10 wt%. The solutions were stirred at room temperature for 24 h before use.

The viscosity of the solutions at different concentrations was measured at room temperature using an Ostwald viscometer (PSL tube viscometer, BS/U type) with a 4 mm capillary. Glycerol (Sigma Aldrich) was used to calibrate the viscometer. To determine the reproducibility and the consistency of the observed viscosity, measurements were repeated twice.

The facility for electrospinning consisted of a glass pipette with controlled orifice diameter varying from 0.1 to 1.2 mm. The set-up for the pump-free electrospinning is shown in Scheme 1. The pipette orifice diameter was measured using optical microscopy and calibrated with a scanning electron microscope (SEM, Jeol JSM820). The fibers were collected on a sheet of earthed aluminum foil, which was placed at a distance ranging from 10 to 20 cm from the end of the pipette. The pipette was mounted horizontally to remove the effect of gravity on the flow rate. A wire, connected to a high voltage DC supply (maximum 50 kV), was directly inserted into the polymer solution loaded inside the pipette, to supply the positive bias. All experiments were carried out at room temperature, stabilized at 22°C, with a relative humidity of 35%.

The diameter and morphology of the collected polymer fibers were studied by SEM operated between 10 and 30 kV. For each electrospun sample, the diameters of 100 fibers were measured in at least 20 different fields and were then averaged. The error bars in the fiber diameter plots correspond to the full width of half maximum (FWHM) of the diameter distribution.

In order to understand the influence of processing parameters individually, and to determine their sensitivity towards the morphology of electrospun polymer fibers, only one parameter at a time was varied while all the other physical parameters were kept constant, in order to supply systematic experimental information which can be used for further theoretical modeling.

2.1 Theoretical considerations

When a charged liquid cylinder within the nozzle is subject to an external electrical field, a pressure is generated

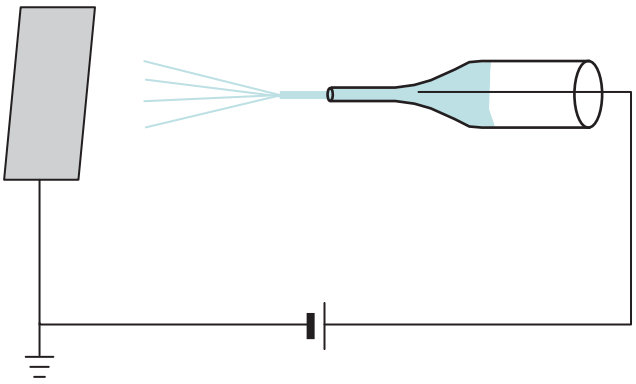

Scheme 1 A typical setup of pump-free electrospinning.

between the solution and the counter electrode. This force acts so as to extract the solution, creating a convex meniscus balanced by the surface tension at the liquid-air-nozzle interface. The equilibrium extracting force, P, formulated by Taylor [27], is described in Eq. (1):

$$P=2\pi RT\cos\phi+W-\pi R^2p \tag{1}$$

where W is the weight of the fluid above the nozzle, p is the pressure applied on the solution within the nozzle, T is the surface tension, ϕ is the angle between fluid surface and nozzle wall, which defines the shape of the meniscus, and R is the radius of the nozzle. In our experiments, W becomes negligible as the pipette is horizontal and p is zero, as the process is pump-free and so the extraction force is only balanced by the surface tension term: $2\pi RT\cos\phi$.

At the tip of the nozzle, the solution can be assumed to be in a cylinder shape. The extraction force applied at the liquid at the tip is [28]:

$$P=V^2\int_0^{\infty}\left[dx/(2h+x)\left[\ln\frac{4x(2h+x)}{R^2}\right]^2\right] \tag{2}$$

where V is the electrical potential at the end of the nozzle, h is the distance between the end of the nozzle and the collector, and x is the position along the axis of the needle. The extraction force is proportional to the V^2, which is due to both the charge density and electrostatic forces being linearly proportional to the applied potential. The integration in Eq. (2) reflects the geometric factors that affect the charge distribution, as well as the attractive interaction between the liquid and collector. When this extraction force is larger than the surface tension of the liquid in the needle, given by $2\pi RT\cos\phi$, the solution will be extracted out of the needle.

Once the solution is extracted from the pipette, it will be stretched into nanofibers, due to the electrical field. This stretching process follows the mass, charge, and momentum conservation laws in concert with stead state fluid dynamic theory, as established by Feng [29]. Mass conservation requires that:

$$\pi r^2v=Q \tag{3}$$

where v is the linear stretching rate, r is the diameter of the fiber and Q is the volume flow rate. In our pump-free process, Q is a function of strength of electrical field, solution viscosity and nozzle diameter. In contrast, for a conventional flow-controlled process, Q is normally assumed to be constant. However, this is not necessarily true if the delivery rate is higher than the flow rate determined by the stretch rate. In such cases, excess solution will be accumulated at the end of the nozzle, in which the concentration will increase due to the solvent evaporation, and control of the solution composition may be lost.

3 Results and discussion

3.1 Viscosity measurements

For a linear polymer like PMMA, the solution viscosity reflects the entanglement of the polymer molecules. Such intermolecular interactions form one of the most critical internal parameters influencing the morphology of the final electrospun material: at very low concentrations and therefore viscosity, cups, rings, and other morphologies are formed instead of fibers [30].

Our measured specific viscosity as a function of PMMA concentration is shown in Figures 1A and 1B. An almost linear dependence of viscosity on PMMA concentration can be found at very low concentrations, which gives an intrinsic viscosity of 145.4 cm^3/g, followed by a nonlinear increase of the viscosity, shown in Figure 1A. This measured intrinsic viscosity of PMMA in DMF is in excellent agreement with the predicted value of 150.3 cm^3/g, using the polymer molecular weight 996,000 g/mol, and Mark-Houwink-Sakurada relationship [31] with parameters from Dobkowski [32].

The logarithmic scale plot, shown in Figure 1B, reveals two different power law dependences in different concentration regions. The intersection of the two concentration dependencies of these regimes yields the critical entanglement concentration, c_e. In our experiments, the point of interaction occurred at a concentration of 3.3 wt%. As c_e represents the point above which significant 3D entanglement dominates the observed viscosity, this concentration is critical in the electrospinning process, as significant

interchain interactions are essential to balance the surface tension. With $c<c_e$, this interaction is too weak to compensate for the surface tension, resulting in droplets rather than fibers. Therefore, for solutions with lower viscosity and higher surface tension, the spinning solution breaks down into droplets, while for solutions with higher viscosity and lower surface tension, fibers can be formed [10].

Quantitative analysis of the two power law behaviors of the viscosity, reveals an exponent of 1.24 for the semidiluted unentangled regime and an exponent of 4.82 for the semidiluted entangled regime. For low concentration solutions, McKee et al. [33] have identified an exponent of 1.25, while for high concentration solutions, Colby et al. [34] predicted the exponent of 4.5 and measured experimentally a value of 4.8. Our measurements are in good agreement with these values. An exponential value for 4.82 corresponds to significant close packing of chains if the Higgins equation is obeyed in this system [35], although Gupta et al. [36] reported the exponents of 0.65 and 5.3 for the two concentration regimes.

3.2 Effect of polymer concentration

The entanglement interactions of polymer chains resist the break-up of the viscoelastic jet into droplets, which leads to formation of long fibers. The morphology and diameter of such spun fibers therefore depends upon the factors that affect the viscosity of solution, such as polymer concentration and molecular weight of the polymer. Since the molecular weight of PMMA is fixed in our study, the viscosity of solution is solely determined by the concentration of the PMMA.

Examples of the concentration-dependent morphology of the electrospun PMMA nanofibers, observed by SEM, are shown in (Figure 2); the scale bars of large size SEM images in Figure 2 are 50 μm, and the inserts show magnified SEM images with scale bars corresponding to 10 μm. In these experiments, all parameters bar the concentration, were fixed: the pipette diameter was 0.4 mm and the distance between the end of the nozzle and the collector was 20 cm with a bias of 20 kV. At a concentration of 1 wt%, which is substantially lower than c_e=3.3 wt%, only polymer droplets were observed (Figure 2A), which is consistent with the theoretical discussion above. The droplets were all in the prolate spheroid shapes, with a longer dimension of approximately 890 nm and the shorter dimension of approximately 300 nm. Such elongated shapes are a direct result of the stretching in the electrical field during the spinning process. Most of the droplets had dimples in the middle, which we attribute to the evaporation of the solvent. The measured flow rate was about 8 ml/h.

At a polymer concentration of 2 wt%, the measured viscosity was about 4.5 mPa s and beaded fibers were formed; images of the spun material at this concentration are shown in Figure 2B. The residual beads between the fibers were in a similar prolate spheroid shape as observed

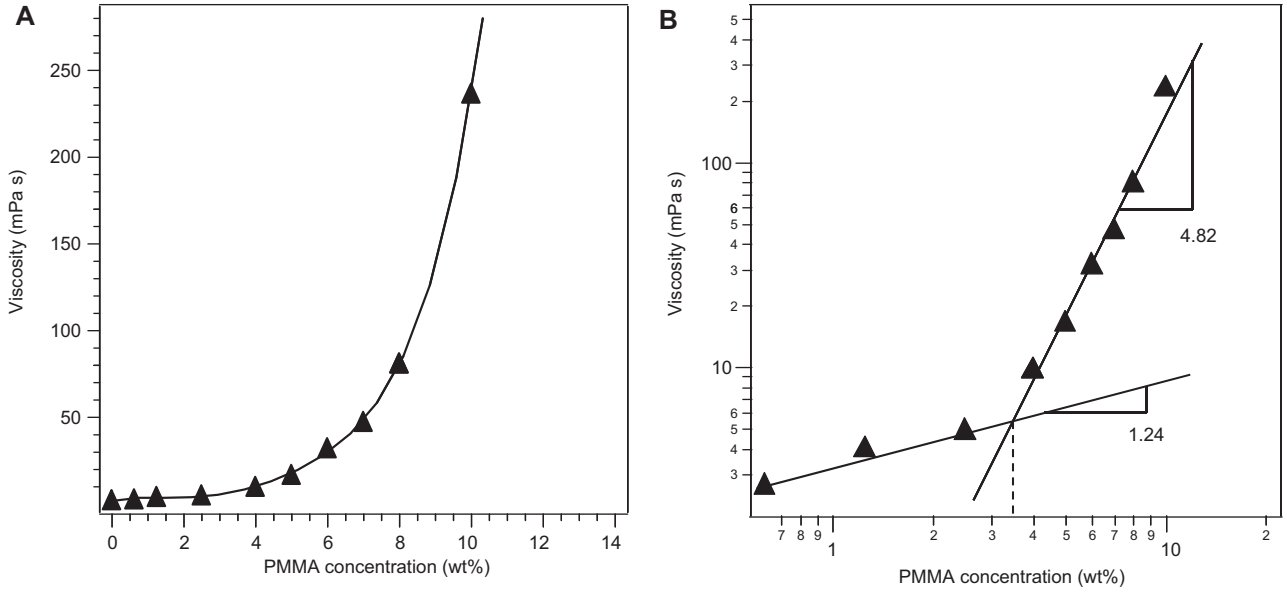

Figure 1 (A) Dependence of solution viscosity as a function of poly(methyl methacrylate) (PMMA) concentration in DMF, (B) plotted on a logarithmic scale with two exponents indicated at different concentrations.

at 1 wt% solution in Figure 2A. The larger droplets (different from beads) were also formed, due to the high flow rate at low viscosity and the measured flow rate for the 2 wt% solution was about 6 ml/h. The average diameter of the fiber was about 88 nm in the bead free sections. At this concentration, the surface tension was balanced by the viscosity when the concentration increased from 1 to 2 wt%. Therefore, both beads and fibers were formed as a mixture of morphologies.

For a polymer concentration of 4 wt%, slightly larger than the c_e (3.3 wt%), the measured viscosity was increased to 9.9 mPa s, indicating stronger interactions between polymer chains. At this viscosity, the measured flow rate was reduced significantly to a level of 3 ml/h. The percentage of the beads was reduced dramatically, while the diameter of the fibers was also increased to 182 nm; images of the spun fibers are shown in Figure 2C.

At 6 wt% solution, shown in Figure 2D, uniform fiber structure was found with far fewer beads, with an average fiber diameter increasing to 294 nm. Further increasing of polymer concentration to 8 wt% provided negligible increases in fiber diameter, although the viscosity increased to 81 mPa s. As the concentration increased to 10 wt%, the viscosity of the solution increased to 236 mPa s. Not only did the average diameter increase to over 900 nm, but the diameter distribution also became much wider in comparison to the fibers spun from 4 to 8 wt% solutions. This is attributed to the fiber splaying and splitting, as shown in the SEM image in Figure 2F. For solutions with PMMA concentration above 6 wt%, a stable flow rate of 1 ml/h was achieved. This corresponds to a minimum flow rate determined by nozzle diameter and field strength.

Shenoy and co-workers [37] reported a semi-empirical analysis to explain the effect of polymer entanglements on the concentration limit for fiber formation. Comparing with experimental results, they reported that with an entanglement number, *ne*, between 2 and 3.5, both fiber and beads were formed; with *ne* larger than 3.5, good quality, bead-free fibers were formed. These entanglement numbers correspond to the concentration limit of 3.1 wt% and 5.4 wt% for PMMA (Mw~996,000 g/mol) solutions in DMF used in this work and the observed formation of bead-free fibers at PMMA concentrations above 6 wt% is in good agreement with the prediction using Wnek's semi-empirical analysis [37].

Figure 3A summarizes the average diameter of the PMMA fibers as a function of polymer concentration. The measured FWHM of the fiber diameter distribution function is shown as the error bars in Figure 3. It is clear that as the concentration increased, both the fiber diameters and their distribution also increased. In particular, a sharp increase of diameter and distribution was found

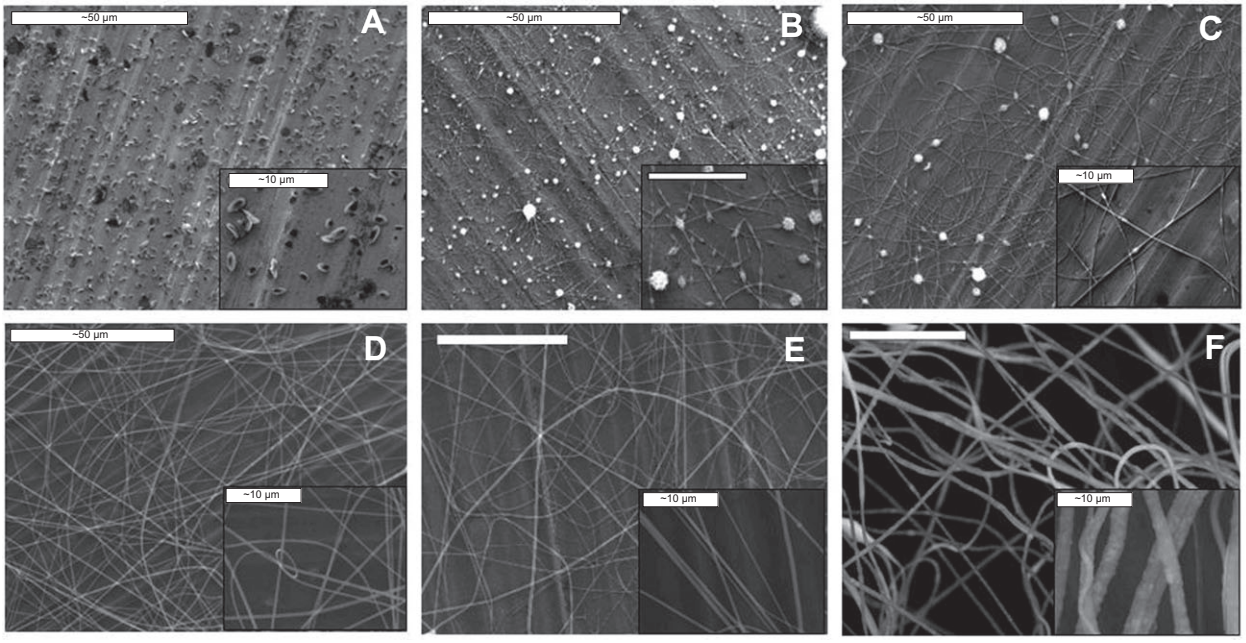

Figure 2 Scanning electron microscopy (SEM) images of poly(methyl methacrylate) (PMMA) electrospun from solution with different concentrations: (A) 1 wt%, (B) 2 wt%, (C) 4 wt%, (D) 6 wt%, (E) 8 wt%, and (F) 10 wt%. The scale bar of the main image corresponds to 50 µm. The inserts show a magnified SEM image with scale bar corresponding to 10 µm.

between 8 and 10 wt%. Overall, a power law relationship with an exponent of 4.2 was observed. Similar behavior was observed by Gupta et al. [36], although an exponent of 3.1 was reported.

In order to understand the quantitative effects of solution viscosity, the fiber diameter was plotted against the measured viscosity (Figure 3B). To our surprise, a good linear relationship with a slope of 3.24 nm/(mPa s) and a R^2 of 0.983 can be identified; Gupta et al. [36] also reported a linear relationship between the fiber diameter and solution viscosity for molecular weight less than 100,000 g/mol, but a power relationship with an exponent of 0.72 for higher molecular weight PMMA solutions. McKee et al. [33] reported power law dependence with an exponent of 0.8. The discrepancy between these observations may be caused by variations in a controlled flow rate in their experiments. In our measurements, the flow rate was naturally determined by the viscosity of the solution, the nozzle diameter and the applied electric field strength. A higher extracting rate was achieved for lower viscosity solutions; as a function of polymer solution concentration, our measured flow rate varied from 8 ml/h (1 wt% PMMA in DMF) to 1 ml/h (6 wt% PMMA in DMF). However, most of the reported work was carried out with a fixed flow rate at 1~2 ml/h. This will restrict the natural formation of the Taylor cone, causing interrupted and delayed electrospinning and resulting in a smaller fiber diameter. Our pump-free process eliminates the restriction of the fixed flow control and reflects the true effects of the viscosity. The identified linear relationship implies the significance of the solution viscosity, which reflects the inter-polymer-chain interactions, on the morphology of the polymer fibers.

3.3 Effect of diameter of pipette orifice

Pipettes with different nozzle diameters were used in order to investigate their effects on the morphology and diameter of the fibers with all other parameters kept constant. The concentration of the solution was 6 wt% and a bias of 20 kV was applied with the collector set at 20 cm from the end of the pipette. Pipette nozzle diameters of 0.1, 0.3, 0.5, 0.7, 1.0, and 1.2 mm were tested. The reason for using a 6 wt% solution is that the best quality fibers are formed at this concentration and the extraction rate in our pump-free process was less dependent on the solution concentration and viscosity.

The results are shown in Figure 4. The results show that it is possible to reduce the diameter of the fibers by reducing the diameter of the pipette orifice. Using a 0.1 mm orifice, uniform fibers with an average diameter of 180 nm were formed. However, using a 1.2 mm pipette orifice, the average fiber diameter was increased to 330 nm with much wider distribution. The plot shows an exponential dependence of the fiber diameter on the nozzle diameter. The fiber diameters show a steeper increase, followed by a relatively flat increase as the nozzle diameter increases from 0.1 mm to 0.8 mm. At a large nozzle diameter, from

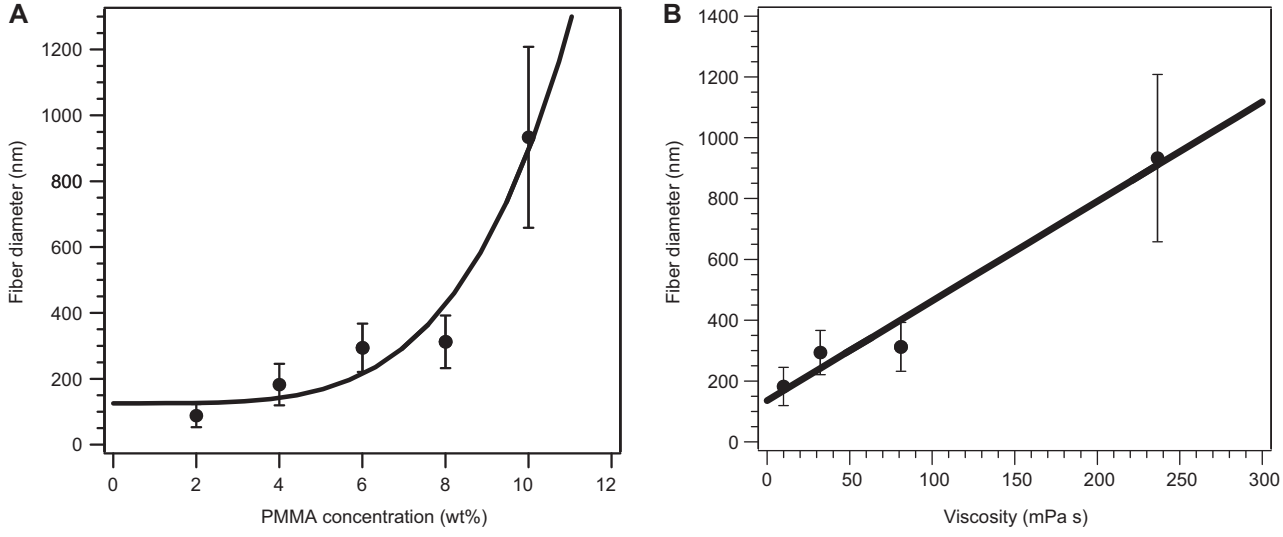

Figure 3 (A) The diameter of electrospun fiber as a function of poly(methyl methacrylate) (PMMA) concentration, (B) the diameter of fiber as a function of solution viscosity. The error bar indicates the full width of half maximum (FWHM) of the distribution function of the fiber diameters.

0.8 mm to 1.2 mm, not only did the average fiber diameter increase, but its distribution also became wider. In such cases, the flow of the solution was no longer restricted by the nozzle diameter.

Our observation is qualitatively in agreement with measurements taken by Katti et al. [17], although in their work, only three data points were presented. In contrast, Macossay et al. [18] reported that the nozzle diameter has no influence on the fiber diameter. The reason for such inconsistent results could also be explained as the effects of flow rate control. When the flow rate is higher than the extraction rate, determined by viscosity, solution charge density, and electric field strength, the nozzle size will have less effect on the fiber diameter, since much of the solution will be accumulated at the end of nozzle. Equally, when the flow rate is lower than the extraction rate, the flow rate itself will not be able to influence the fiber diameter, which was observed by Tan et al. [38]. Therefore, only when the volume feed rate matches the extraction rate can the reliable fiber diameter dependence on the nozzle size be quantitatively measured. The most effective way to achieve such conditions is to eliminate the external flow rate control, in other words, to use pump-free electrospinning. In this case, it is expected that the size of the Taylor cone base is determined by the orifice diameter of the nozzle only, which in turn affects the surface charge density, the diameter of the jet, and ultimately the diameter of the fibers.

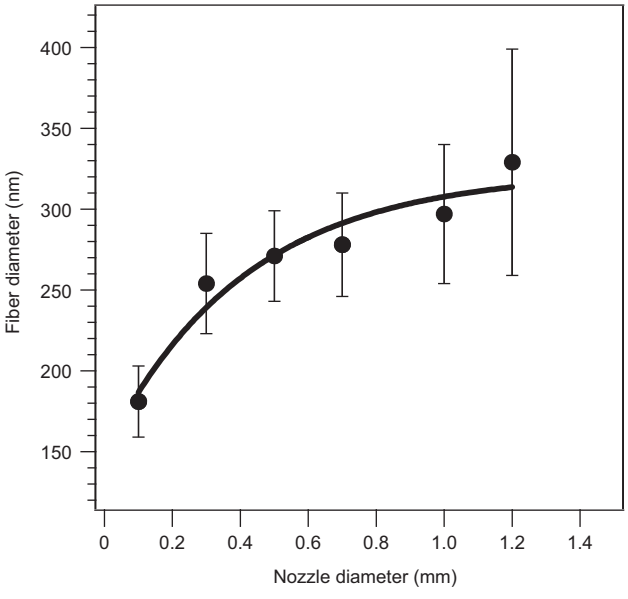

Figure 4 Dependence of measured fiber diameter on the nozzle diameter for electrospinning. The error bars show the fiber diameter distribution.

3.4 Effect of applied bias

The voltage dependence of fiber diameter was also studied using a solution with a PMMA concentration of 6 wt%, a fixed nozzle diameter of 0.4 mm, and a fixed distance between the collector and pipette of 20 cm. Within the voltage range of 10–30 kV, good quality polymer fibers were produced and the observed diameter versus bias is plotted in Figure 5. Increasing the electrospinning voltage caused a small increase in the nanofiber diameter from 290 nm at 10 kV to 308 nm at 30 kV. The observed bias-dependent fiber diameter followed a nonlinear relationship, reflecting that, at higher bias, the fiber diameter increased more rapidly.

The positive voltage bias drives the charged jet to emerge from the tip through the Taylor cone rapidly, when the high electrostatic forces overcome the viscosity. In other words, with fixed diameter and collector position, the higher bias caused a faster extraction rate and therefore, larger fiber diameters. Our measurement has shown at 10 kV, that the measured extraction rate is about 0.8 ml/h, which increases to 1 ml/h at 20 kV and 3 ml/h at 30 kV. Although our voltage-dependent results are generally in good agreement with the literature [19, 20, 38], several inconsistent results have also been reported. For instance, Katti et al. [17] reported that an increase in voltage caused a decrease in nanofiber diameter initially, and further increase in the voltage caused fluctuation of the nanofiber diameter. More controversially, measurement taken by Gu et al. [21] showed no correlation between fiber diameter and bias voltage. Moreover, careful inspection of the data reported by Zhang et al. [19] and Nasir et al. [20] also revealed a sublinear curvature, whereas our results show a superlinear curvature. Such a complex spectrum of the voltage-dependent results should be thoroughly analyzed, in order to obtain a comprehensive understanding of the whole picture, although it is worth mentioning that most of these reported results are obtained using flow control. As we have explained above, flow rate limit on the extraction rate could be the origin of these contradictory results. With a controlled low flow rate, the effects of increasing bias will cause changes in the shape and size of the Taylor cone, rather than affect the diameter of the resulting fibers.

The extraction force on the solution is proportional to V^2, at a bias of V, as described in Eq. (2), and so is the flow rate. Therefore, the diameter of the nanofibers increases. The increase in the fiber diameter is also accompanied by increasing diameter distribution (Figure 5). The increased breadth of the distribution could be due to splitting and splaying of the polymer

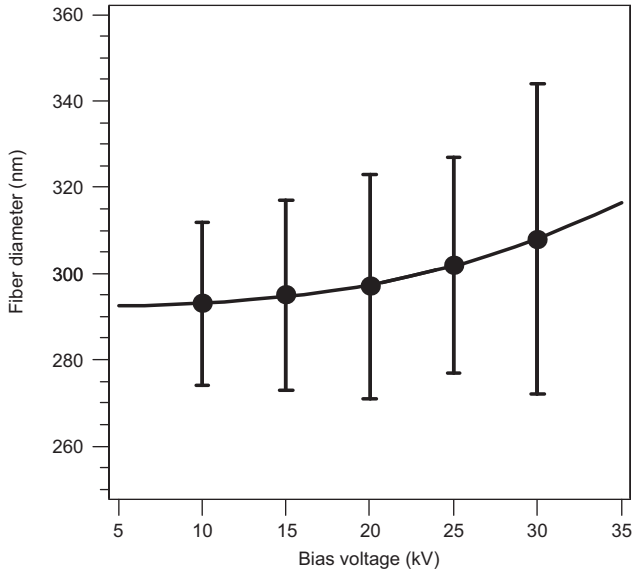

Figure 5 Dependence of fiber diameter on the bias voltage applied between the electrospinning nozzle and the collector.

fibers, due to the high ejection rate at higher bias (above 20 kV). We also observed the increase in bead production at high electric potential.

3.5 Effect of distance between the nozzle and the collector

With fixed solution concentration (6 wt%), bias voltage (20 kV), and nozzle diameter (0.4 mm), the fiber diameters were measured as a function of the distance between the end of the pipette and the collector (Figure 6). While the bias applied could affect both the charge density and the fiber thinning process, the distance between the pipette and collector would only affect the thinning and whipping process. Therefore, it is necessary to distinguish between the effects of bias and the effects of distance between the nozzle and the collector. Between 10 cm and 20 cm, high quality uniform and bead-free fibers were formed, while the fiber diameter decreases when the distance increases, following an inverse relationship.

Similar to decreasing bias voltage, increasing collector distance will reduce the electric field strength. Thus the fiber diameter will be expected to decrease, with an improved fiber quality. Meanwhile, the increase in distance provides more time for the thinning process arising from the whipping instability, which also results in finer fibers with a narrower diameter distribution. In our experiment, it is difficult to quantitatively distinguish the contribution of electric field strength from the fiber thinning process. Further experiments will be carried out to maintain the strength of the electric field by compensating with a higher bias at a larger distance, so only the contribution from the thinning time can be measured.

4 Conclusions

The effects of critical extrinsic processing parameters, including viscosity, concentration, nozzle diameter, voltage bias, and nozzle to collector distance, on the diameter and morphology of electrospun PMMA fibers, were investigated. Having recognized the significant effects of the flow rate on the dependence of other processing parameters, we investigated a pump-free electrospinning process. This study showed that, in the absence of mechanical pumping and flow control, the morphology and diameter of nanofibers can be controlled and their formation can be understood at a fundamental level. This technique can be used for further detailed experimental and theoretical study of electrospinning.

The viscosity of the PMMA solution was measured as a function of solution concentration, with excellent agreement with that predicted by the Mark-Houwink-Sakurada relationship. The critical entanglement concentration c_e=3.3 wt% was identified. More importantly for the fiber diameter, the viscosity dependence showed a linear

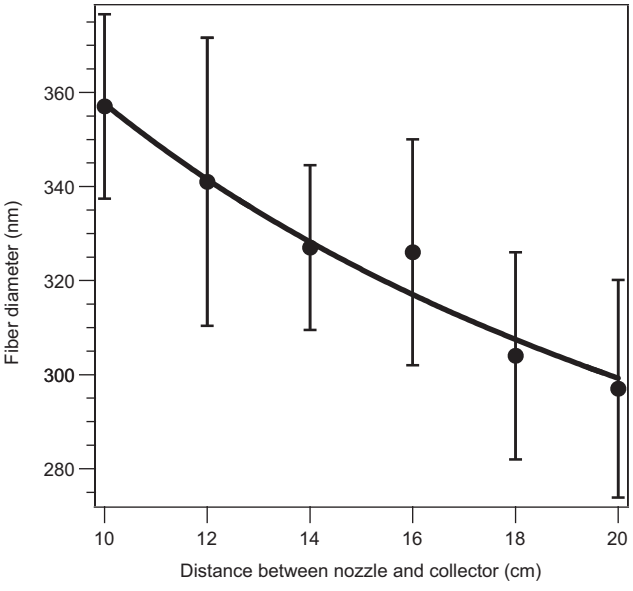

Figure 6 The measured fiber diameter as a function of distance between the nozzle and the collector.

relationship. The interference of flow control on the viscosity dependence is also discussed.

With fixed concentration, the fiber diameter dependence on the processing parameters, including nozzle diameter, voltage bias and nozzle to collector distance, was quantitatively analyzed. Decreasing the nozzle diameter can reduce the fiber diameter significantly with improved quality, following an exponential relationship. The bias dependence showed that decreasing the bias will reduce the average diameter and give a narrower distribution, following a power law. Similarly, increasing the distance between the end of the nozzle and the collector, can also reduce the fiber diameter. An inverse dependence of fiber diameter on the nozzle to collector distance has been found as the best fitting. The mechanism of flow rate restriction, forming of the Taylor cone, fiber thinning, and how they affect the nanofiber diameter, were discussed.

Acknowledgments: The project is supported by EPSRC CASE award. QC thanks Dr. S. Firth at University College London for donating the Jeol JSM820 SEM. QC also thanks Professor Norman Billingham for detailed discussion on the rheology properties of polymer solutions. JSB gratefully acknowledges the Commonwealth Scholarship Commission for his scholarship. JFCT acknowledges the support of EU Marie-Curie Actions and the ERC. The authors would like to thank PpTek Ltd. for supporting the project.

Received August 16, 2012; accepted May 20, 2013; previously published online June 18, 2013

References

[1] Choi SW, Jo SM, Lee WS, Kim YR. *Adv. Mater.* 2003, 15, 2027–2032.
[2] Xu SY, Shi Y, Kim SG. *Nanotechnology* 2006, 17, 4497–4501.
[3] Subbiah T, Bhat GS, Tock RW, Pararneswaran S, Ramkumar SS. *J. Appl. Polym. Sci.* 2005, 96, 557–569.
[4] Welle A, Kroger M, Doring M, Niederer K, Pindel E, Chronakis S. *Biomaterials* 2007, 28, 2211–2219.
[5] Francis L, Nair AS, Jose R, Ramakrishna S, Thavasi V, Marsano E. *Energy* 2011, 36, 627–632.
[6] Liu RL, Ye HY, Xiong XP, Liu HQ. *Mater. Chem. Phys.* 2010, 121, 432–439.
[7] Pedicini A, Farris RJ. *J. Polym. Sci., Part B: Polym. Phys.* 2004, 42, 752–757.
[8] Deitzel JM, Kosik W, McKnight SH, Tan NCB, DeSimone JM, Crette S. *Polymer* 2002, 43, 1025–1029.
[9] Kim ID, Rothschild A. *Polym. Adv. Technol.* 2011, 22, 318–325.
[10] Zeleny J. *Phys. Rev.* 1914, 3, 69–91.
[11] Fong H, Chun I, Reneker DH. *Polymer* 1999, 40, 4585–4592.
[12] Bognitzki M, Czado W, Frese T, Schaper A, Hellwig M, Steinhart M, Greiner A, Wendorff JH. *Adv. Mater.* 2001, 13, 70–72.
[13] Lee KH, Kim HY, La YM, Lee DR, Sung NH. *J. Polym. Sci. Part B: Polym. Phys.* 2002, 40, 2259–2268.
[14] Doshi J, Reneker DH. *J. Electrost.* 1995, 35, 151–160.
[15] Baumgart PK. *J. Colloid Interface Sci.* 1971, 36, 71–79.
[16] Reneker DH, Yarin AL, Fong H, Koombhongse S. *J. Appl. Phys.* 2000, 87, 4531–4547.
[17] Katti DS, Robinson KW, Ko FK, Laurencin CT. *J. Biomed. Mater. Res., Part B Appl. Biomaterials* 2004, 70B, 286–296.
[18] Macossay J, Marruffo A, Rincon R, Eubanks T, Kuang A. *Polym. Adv. Technol.* 2007, 18, 180–183.
[19] Zhang CX, Yuan XY, Wu LL, Han Y, Sheng J. *Eur. Polym. J.* 2005, 41, 423–432.
[20] Nasir M, Matsumoto H, Danno T, Minagawa M, Irisawa T, Shioya M, Tanioka A. *J. Polym. Sci., Part B: Polym. Phys.* 2006, 44, 779–786.
[21] Gu SY, Ren J, Vancso GJ. *Eur. Polym. J.* 2005, 41, 2559–2568.
[22] Demir MM, Yilgor I, Yilgor E, Erman B. *Polymer* 2002, 43, 3303–3309.
[23] Dahlin RL, Kasper FK, Mikos AG. *Tissue Eng. Part B:Rev.* 2011, 17, 349–364.
[24] Liu Y, Ji Y, Ghosh K, Clark RAF, Huang L, Rafailovichz MH. *J. Biomed. Mater. Res. Part A* 2009, 90A, 1092–1106.
[25] Miao JJ, Pangule RC, Paskaleva EE, Hwang EE, Kane RS, Linhardt RJ, Dordick JS. *Biomaterials* 2011, 32, 9557–9567.
[26] Gao DW, Wang QQ, Qiao H, Cai YB, Huang FL, Wei QF. *J. Eng. Fibers Fabr.* 2012, 7, 94–98.
[27] Taylor G. *Proc. R. Soc. London Ser. A-Math. Phys. Sci.* 1969, 313, 453–470.
[28] Vandyke MD. *Proc. R. Soc. London Ser. A-Math. Phys. Sci.* 1969, 313, 471–475.
[29] Feng JJ. *Phys. Fluids* 2002, 14, 3912–3926.
[30] Wang HG, Liu QW, Yang QB, Li YC, Wang W, Sun L, Zhang CQ, Li YX. *J. Mater. Sci.* 2010, 45, 1032–1038.
[31] Tanford C. *Physical Chemistry of Macromolecules*, John Wiley & Sons: New York, 1961.
[32] Dobkowski Z. *Polimery* 1984, 29, 238–241.
[33] McKee MG, Wilkes GL, Colby RH, Long TE. *Macromolecules* 2004, 37, 1760–1767.
[34] Colby RH, Fetters LJ, Funk WG, Graessley WW. *Macromolecules* 1991, 24, 3873–3882.
[35] Matsuoka S, Cowman MK. *Polymer* 2002, 43, 3447–3453.
[36] Gupta P, Elkins C, Long TE, Wilkes GL. *Polymer* 2005, 46, 4799–4810.
[37] Shenoy SL, Bates WD, Frisch HL, Wnek GE. *Polymer* 2005, 46, 3372–3384.
[38] Tan SH, Inai R, Kotaki M, Ramakrishna S. *Polymer* 2005, 46, 6128–6134.